Structural and Multidisciplinary Optimization (2018) 58:2325–2340
https://doi.org/10.1007/s00158-018-2077-1

RESEARCH PAPER

Efficient global sensitivity analysis with correlated variables

Erin C. DeCarlo[1] · Sankaran Mahadevan[1] · Benjamin P. Smarslok[2]

Received: 22 September 2017 / Revised: 14 August 2018 / Accepted: 20 August 2018 / Published online: 26 October 2018

Abstract

Existing methods for the computation of global sensitivity indices are challenged by both number of input-output samples required and the presence of dependent or correlated variables. First, a methodology is developed to increase the efficiency of sensitivity computations with independent variables by incorporating optimal space-filling quasi-random sequences into an existing importance sampling-based kernel regression sensitivity method. Two prominent situations where parameter correlations cannot be ignored, however, are (1) posterior distributions of calibrated parameters and (2) transient, coupled simulations. Therefore, the sensitivity methodology is generalized to dependent variables allowing for efficient post-calibration sensitivity analyses using input-output samples obtained directly from Bayesian calibration. These methods are illustrated using coupled, aerothermal simulations where it is observed that model errors and parameter correlations control the sensitivity estimates until coupling effects become dominant over time.

Keywords Global sensitivity analysis · Correlated parameters · Sobol' indices · Bayesian calibration · Importance sampling · Kernel regression

Nomenclature

D	Dimension of input space
h	Bandwidth of Gaussian kernel
K	Kernel function
M	Number of model evaluations
N	Number of sensitivity iterations
p	Probability density function
Q	Heat flux (W/m^2)
$S_{d,1}$	First-order effect of parameter X^d
$S_{d,T}$	Total effects of parameter X^d
t	Time
T	Temperature (K)
x	Model input
X^d	Samples for d^{th} input dimension
$\boldsymbol{X}^{\sim d}$	Samples for all but d^{th} input dimension
y	Model output
Y	Vector of M model outputs
δ	Aerothermal model discrepancy
ε	Model discrepancy
Δt	Time step
θ	Model parameter
μ	Mean
σ^2	Variance

Subscripts

0	IInitial condition
1	1st model in a series
2	2nd model in a series
4	Panel location
d	Input dimension index
f	Final time of interest
i	i^{th} outer loop sensitivity iteration
j	j^{th} model evaluation or inner loop sensitivity iteration
t	Time index
X^d	Statistic of X^d
$\boldsymbol{X}^{\sim d}$	Statistic of $\boldsymbol{X}^{\sim d}$

Superscripts

d	d^{th} input dimension

Responsible Editor: Jose Herskovits

✉ Erin C. DeCarlo
ecdecarlo@gmail.com

[1] Department of Civil & Environmental Engineering, Vanderbilt University, Nashville, TN 37235, USA

[2] Aerospace Systems Directorate, Structural Sciences Center, Air Force Research Laboratory, Wright-Patterson AFB, Dayton, OH 45433, USA

1 Introduction

Uncertainty inherently exists in physical systems due to both random variations and limited states of knowledge that include (1) natural variability in system inputs (e.g., materials, geometry, fluid properties, and loading); (2) uncertainty from measurement errors and limited data; and (3) and model uncertainty and errors from simplified or poorly understood physics, their interactions, and numerical approximations (Sankararaman 2012). The focus of this paper is global sensitivity analysis (GSA) which provides useful insights into both the forward problem of uncertainty propagation and the inverse problem of uncertainty reduction by quantifying how predictions are influenced by individual uncertainty sources. In addition, GSA supplements decision-making for targeting critical sources of uncertainty with additional testing to improve overall prediction confidence.

The inclusion of uncertainty in multidisciplinary analyses (MDA) has led to significant research in robust multidisciplinary design optimization approaches which require quantifying how the system performance is affected by individual sources of uncertainty (Hu and Du 2013; Hu and Mahadevan 2015; Liang and Mahadevan 2015, 2016). Sensitivity analyses for MDA and MDO for forward problems of uncertainty quantification (UQ) have largely focused on local gradient-based sensitivities to find local optima in the design space. In contrast to gradient-based sensitivities at a chosen nominal or design value, GSA uses the entire probability distribution of the uncertainty sources for variance-based sensitivity estimates. Sobol' indices are a set of variance-based global sensitivity indices that quantify both individual and interactive effects between uncertain parameters on the prediction variance (Sobol' 2001). The interactive effects are especially important in multidisciplinary simulations where parameter interactions among multiple disciplinary models may contribute to additional uncertainty in the predicted response (Mahadevan and Liang 2011).

Sobol' indices for GSA present computational challenges, however, due to the large number of input-output samples needed to estimate the uncertainty contributions from even a single variable and quickly become intractable as the number of uncertain parameters increases. A widely used class of matrix methods (Saltelli et al. 2008) has improved the computational efficiency of calculating both the first-order and total effects indices; however, the computational burden may still be too large for problems with expensive models. To alleviate the computational burden of GSA and other uncertainty quantification methods, surrogate models have been used in place of expensive simulations (Cukier et al. 1973; Ratto et al. 2007). However, the additional step of training and validating a surrogate to get accurate predictions is not straightforward and is dependent on the set of training points and the dimension of the input parameter space. Hu and Mahadevan (2016) recently investigated global sensitivity analysis-enhanced surrogate (GSAS) modeling for reliability analysis where the new training points for surrogate construction are selected based on GSA results; however, this further motivates more efficient GSA computations that are not reliant on a surrogate model.

Other works have focused on efficiently using existing sets of input-output samples from model verification, validation, or calibration stages of model development. For example, Li and Mahadevan (2016) developed a modular global sensitivity analysis methodology that uses stratified sampling to assign uniform weights to one-dimensional strata for computing first-order Sobol' indices. Efficient sensitivity analysis from a fixed sample set has also been explored by Jia and Taflanidis (2016) using an auxiliary probability density function (PDF) of the samples and estimating the sensitivities from marginal densities constructed via kernel density estimation. A similar idea has been explored using an importance sampling-based kernel regression method (ISK-GSA) developed by Sparkman et al. (Sparkman et al. 2016) where the choice of kernel need not be uniform and can follow the distribution type of the parameter. Furthermore, the ISK-GSA method calculates Sobol' indices in fewer model runs and has the desired capability of additionally being able to efficiently compute the total effects Sobol' indices using the same existing input-output samples. Thus, the ISK-GSA methodology provides the foundation for the research contributions presented in this paper.

For inverse problems in UQ, GSA is used to identify the subset of uncertain inputs and parameters that are candidates for uncertainty reduction through calibration. Bayesian model calibration has been pursued for aerothermoelastic model components in related work (Smarslok et al. 2012; DeCarlo et al. 2013, 2014, 2016) and performed using sampling methods (e.g., Markov chain Monte Carlo (Hastings 1970), slice sampling (Neal 2003), or particle-filtering (Kostanjčar et al. 2009)). Calibration requires a significant number of model evaluations, the posterior distributions converge; however, these input-output samples cannot be integrated into downstream sensitivity analyses since the posterior distributions of the parameters exhibit correlation. In the literature, GSA with dependent variables is typically consigned to either expensive double-loop computations, grouping the correlated parameters into one auxiliary variable (Liang et al. 2015), or a combination of both approaches. As such, the input-output samples from calibration have yet to be efficiently integrated into post-calibration GSA and is a significant research gap that is addressed with the proposed methodology.

First, the proposed methodology addresses independent variables and improves the ISK-GSA methodology developed by Sparkman et al. (2016) by using quasi-random sequences. Studies have found that quasi-random sequences provide optimal space-filling designs in higher dimensions (Camberos et al. 2007) and the combined methodologies improve the convergence in estimating the sensitivity of a model output to independent sources of uncertainty. Second, the ISK-GSA method is generalized to allow consideration of dependent

variables which are observed (a) in posterior samples of calibrated parameters and (b) among parameters and model outputs passing between coupled models in MDA.

The outline of this paper is as follows: Sobol' indices for global sensitivity analyses are presented in section 2.1 followed by an overview of the ISK-GSA method as developed by Sparkman et al. in section 2.2. Section 3.1 presents the proposed methodology suitable for independent variables that uses space-filling quasi-random number generators together with the ISK-GSA method. In section 3.2, the generalized ISK-GSA methodology is developed to handle dependent variables which are observed after calibration and between coupled models through time and is demonstrated on an illustrative time-dependent example in section 3.3. Section 4 applies the generalized ISK-GSA methodology to compute the posterior GSA results through time for a coupled, time-dependent aerothermal analysis and demonstrates the effects of model coupling and parameter correlation on the sensitivity estimates.

2 Global sensitivity analysis methodology

2.1 Sobol' sensitivity indices

The basis of the Sobol' sensitivities indices is found in the variance decomposition theorem shown in Eq. (1). For a model Y,with D number of inputs $\boldsymbol{X}_{1xD}$, the variance decomposition theorem states that the total variance of the model output $Var(Y)$ can be decomposed into the summation of (a) the variance of the expectation of model output conditioned on the d^{th} input variable X^d ($d = 1$ to D) with all other variables $\boldsymbol{X}^{\sim d}$ varying and (b) the expectation of the variance of Y conditioned the same set (Sobol' 2001; Saltelli et al. 2008).

$$Var(Y) = Var_{X^d}\left\{E_{X^{\sim d}}\left[Y|X^d\right]\right\} + E_{X^d}\left\{Var_{X^{\sim d}}\left[Y|X^d\right]\right\} \quad (1)$$

The Sobol' indices are separated into two sets of effects: first-order and total effects. The first-order Sobol' index $S_{d,1}$ is shown in Eq. (2) and is computed as the ratio of variance contributed by the individual variable X^d to the total variance in the output $Var(Y)$.

$$S_{d,1} = \frac{Var_{X^d}\left\{E_{X^{\sim d}}\left[Y|X^d\right]\right\}}{Var(Y)} \quad (2)$$

Note that the numerator of the first-order index in Eq. (2) is the first term on the right-hand side of Eq. (1) while the denominator is $Var(Y)$ is from the left-hand side. This implies that if the contribution of variance from variable X^d is equal to the total variance, its first-order Sobol' sensitivity index is 1 which is the upper bound of the sum of the first-order Sobol' indices across all D dimensions.

The most straightforward and widely used procedure to compute Sobol' indices is the double-loop (DL) method (also referred to as the Sobol' method). In the double-loop method, computing the first-order Sobol' index of variable X^d in Eq. (2) first consists of an outer loop each at a fixed input x_i^d ($i = 1$ to N_{outer}), and an inner loop over $\boldsymbol{x}_j^{\sim d}$ ($j = 1$ to N_{inner}). Within the inner loop, an estimate of the conditional expectation $E_{\boldsymbol{X}^{\sim d}}[Y|X^d = x_i^d]$ is obtained using N_{inner} samples of $\boldsymbol{X}^{\sim d}$. This process is repeated by resampling X^d for each outer loop iteration and the variance of the conditional expectations from each choice of x_i^d is computed as the numerator of Eq. (2).

In contrast, as stated previously, the sum of the first-order indices across all D dimensions is equal to one; however, this applies to the specific scenario of independent inputs with no inherent model interaction. In contrast, the sum of the first-order indices is less than 1 when parameter interactions are significant (either via statistical dependence or model interactions) which are not captured in the first-order Sobol' index.

The total effects Sobol' index $S_{d,T}$ inherently accounts for the first-order effects of X^d as well as the effects of interactions between X^d and all other variables $\boldsymbol{X}^{\sim d}$. Parameter interactions may either be a result of nonlinearities intrinsic to the model, statistical correlations between the parameters in the input space, or a combination of both effects. Statistical correlations may lead to sums of first-order effects larger than 1 or total effects smaller than first-order effects. The total effects indices in Eq. (3) are derived by dividing the second term in Eq. (1) by $Var(Y)$.

$$\begin{aligned} S_{d,T} &= \frac{E_{X^{\sim d}}\left\{Var_{X^d}\left[Y|X^{\sim d}\right]\right\}}{Var(Y)} \\ &= 1 - \frac{Var_{X^{\sim d}}\left\{E_{X^d}\left[Y|X^{\sim d}\right]\right\}}{Var(Y)} \end{aligned} \quad (3)$$

Using the double-loop method and assuming $N_{\text{outer}} = N_{\text{inner}} = N$, the number of total model evaluations M required for estimating both first-order and total effects Sobol' indices for D input parameters is on the order of $O(2DN^2)$), which quickly becomes intractable. The computational expense of GSA was addressed by Saltelli et al. (2008) where a class of matrix column exchange (MCE) methods (also called pick-and-freeze methods (Gamboa et al. 2016)) was developed to simplify GSA by approximating the variances in the numerators. In contrast to the double-loop method for computing Sobol' indices, MCE methods require $M \sim O((2+2D)N)$ to quantify both first-order and total effects.

To implement the MCE method for GSA, first, an initial input matrix of dimension $2N$xD is subdivided into two NxD matrices, $\boldsymbol{X}_A$ and $\boldsymbol{X}_B$. These two input matrices are then propagated through the model for y_A and y_B. Next, a matrix $\boldsymbol{X}_{AB}{}^d$ for each dimension d is then formed by replacing the d^{th} column of $\boldsymbol{X}_A$ with the d^{th} column of $\boldsymbol{X}_B$ such

that $\boldsymbol{X}_{AB}{}^{d} = [\boldsymbol{X}_{A}{}^{1},\ldots \boldsymbol{X}_{A}{}^{d-1}, \boldsymbol{X}_{B}{}^{d},\ldots, \boldsymbol{X}_{A}{}^{D}]$. Each $\boldsymbol{X}_A$, $\boldsymbol{X}_B$, and $\boldsymbol{X}_{AB}{}^{d}$ ($d=$ 1 to D) are propagated through the model for output matrices y_A, y_B, and $y_{AB}{}^{d}$ ($d=$ 1 to D), respectively. Several variance formulations have been explored to use MCE methods for Sobol' indices, which are found via correlation between y_A and $y_{BA}{}^{d}$ (totals) and y_B and $y_{BA}{}^{d}$ (first-order) in the approaches from (Saltelli et al. 2010), respectively, and are presented below in Eqs. (4) and (5).

$$Var_{X^d}\left\{E_{X^{\sim d}}\left[Y|X^d\right]\right\} = \frac{1}{N-1}\sum_{n=1}^{N} y_{A,n}y_{BA,n}^{d} - \frac{1}{N}\sum_{n=1}^{N} y_{A,n}y_{B,n} \quad (4)$$

$$Var_{X^{\sim d}}\left\{E_{X^d}\left[Y|X^{\sim d}\right]\right\} = \frac{1}{N-1}\sum_{n=1}^{N} y_{A,n}y_{AB,n}^{d} - \frac{1}{N}\sum_{n=1}^{N} \left(y_{A,n}\right)^2 \quad (5)$$

Note that GSA methods presented throughout this paper are not conditioned on any one type of model (e.g., data-driven, physics-based, statistical); however, a relationship between inputs and an output quantity of interest does need to be established before a global sensitivity analysis can be conducted. In particular, a challenge with computing Sobol' indices for multidisciplinary analyses with either the DL or MCE methods is two-fold: (1) convergence of the sensitivity estimate is slow from suboptimal sampling and expensive models and (2) MCE methods in particular have difficulty accommodating correlated quantities (Kucherenko et al. 2012; Mara and Tarantola 2012). These challenges are addressed with the proposed GSA methodology in the following sections; however, first, the ISK-GSA methodology is presented to establish notation, terminology, and the state-of-the-art.

2.2 Importance sampling-based kernel regression estimator for Sobol' indices

First, the concepts of kernel regression and importance sampling are introduced without the context of GSA. Then, the formulation of the ISK-GSA methodology that incorporates both kernel regression and importance sampling is presented and compared against DL and MCE methods on the grounds of efficiency.

Consider M available model evaluations are made available with input-output relationships X_{MxD} and Y_{Mx1}. The goal is to make use of these model evaluations in GSA without running more analyses. Therefore, for each existing model evaluation $m=1$ to M and input dimension $d=1$ to D, an estimate of the conditional expectation $E_{X\sim d}\left[Y\,|X^d = x_m{}^{d}\right]$ is achieved by weighting each model output Y as shown in Eq. (6).

$$E_{X^{\sim d}}\left[Y|X^d = x_m^d\right] = \sum_{j=1}^{M} y_j w_j^d \quad (6)$$

The conditional expectation in Eq. (6) is then substituted into the numerator of Eq. (2) to estimate the first-order Sobol' indices of each input variable. Presented further in this section are three methods that can be used to determine the weights $w_j{}^{d}$ in Eq. (6): kernel regression, importance sampling, and ISK-GSA.

2.2.1 Kernel regression weights

Kernel regression uses a locally weighted average within the one-dimensional neighborhood of $x_m{}^{d}$ to compute the first-order index weights. The neighborhood is defined using a univariate kernel function $K_d(x_m{}^{d}\text{-}x_j{}^{d})$ centered around on $x_m{}^{d}$. The kernel function outputs are normalized according to Eq. (7) to define the weights $w_j{}^{d}$ that are used in Eq. (6).

$$w_j^d = \frac{K_d\left(x_m^d - x_j^d\right)}{\sum_{j=1}^{M} K_d\left(x_m^d - x_j^d\right)} \quad (7)$$

Kernel functions can be uniform across all sample points (resulting in a global average), constant for all $x_j{}^{d}$ within a certain squared Euclidean distance $h_d{}^{2}$ from $x_m{}^{d}$, or parametrized as continuous functions that decreases over the distance between the kernel center $x_m{}^{d}$ and $x_j{}^{d}$, such with a Gaussian kernel.

In this work, Gaussian kernels are used and defined with kernel center $c_d = x_m{}^{d}$ and bandwidth $h_d = 1.06\sigma_d\, M^{-1/5}$ (as suggested for Gaussian kernels (Sparkman et al. 2016)) where σ_d is the univariate standard deviation of the samples X^d. Thus, the kernel bandwidth in each dimension d scales linearly with sample variance σ_d and decreases as the number of model evaluations M increases. This implies that as M increases, the conditional expectation estimate around $x_m{}^{d}$ in Eq. (6) can become more localized. The local expectation estimates within the global probability space are supplemented with concepts from importance sampling which are discussed next.

2.2.2 Importance sampling weights

Importance sampling is a variance reduction technique used in engineering reliability analysis that distinguishes between the sampling density $S_{\boldsymbol{D}}(\boldsymbol{x})$ of the input space from which model evaluations or data are generated (e.g., failure region) and a target density $T_{\boldsymbol{D}}(\boldsymbol{x})$ from which statistics are desired (e.g., probability of failure) (Haldar and Mahadevan 2000). Importance sampling comes from the idea that if samples are generated in a region of interest $S_{\boldsymbol{D}}(\boldsymbol{x})$, they can be reweighted to make an assessment about the outcome over the entire probability space of the inputs $T_{\boldsymbol{D}}(\boldsymbol{x})$ according to the likelihood ratio $T_{\boldsymbol{D}}(\boldsymbol{x})/S_{\boldsymbol{D}}(\boldsymbol{x})$.

Therefore, for first-order effects, an estimate within a univariate target region $T_d(x^d)$ using samples from the univariate sampling density $S_d(x^d)$ is achieved using normalized importance sampling weights w_j^d defined according to Eq. (8).

$$w_j^d = \frac{T_d\left(x_j^d\right)/S_d\left(x_j^d\right)}{\sum_{j=1}^{M} T_d\left(x_j^d\right)/S_d\left(x_j^d\right)} \tag{8}$$

For kernel regression weights, however, it is the sampling density that is over the entire probability space and the target density for which the statistics (i.e., conditional means and variances) are to be computed.

2.2.3 Importance sampling-based kernel regression weights

The formulation for the importance sampling-based weights for first-order effects using ISK-GSA arises out of equating the kernel function $K_d(x_m^d\text{-}x_j^d)$ in Eq. (7) that defines the neighborhood around x_m^d and the marginal target density $T_d(\boldsymbol{x})$ from Eq. (8). Likewise, the univariate sampling density $S_d(x^d)$ is equivalent to the marginal probability density of the available inputs $p_d(x^d)$ in each input dimension. Thus, for each model evaluation M, the conditional expectation in Eq. (6) for first-order effects is estimated using the ISK-GSA weights in Eq. (9).

$$w_j^d = \frac{K_d\left(x_m^d - x_j^d\right)/p_d\left(x_j^d\right)}{\sum_{j=1}^{M} K_d\left(x_m^d - x_j^d\right)/p_d\left(x_j^d\right)} \tag{9}$$

Thus far, only univariate weights have been presented for kernel regression, importance sampling, and ISK-GSA. Since kernels can be multidimensional, the theory of these methods is easily extendable to multidimensional input, and thus ISK-GSA method can readily compute total effects Sobol' indices. The conditional expectation for the total effects Sobol' index in the numerator of the second term in Eq. (3) is shown in the form of a weighted sum in Eq. (10). The weights $w_j^{\sim d}$ are computed using Eq. (11) as the multivariate extension of Eq. (9) where $K_{\sim d}(\boldsymbol{x}_m^{\sim d}\text{-}\boldsymbol{x}_j^{\sim d})$ is defined as the D-1 dimensional neighborhood around $\boldsymbol{x}_m^{\sim d}$ (which may be sparse in high dimensions).

$$E_{X^d}\left[Y|X^{\sim d} = x_m^{\sim d}\right] = \sum_{j=1}^{M} y_j w_j^{\sim d} \tag{10}$$

$$w_j^{\sim d} = \frac{K_{\sim d}\left(x_m^{\sim d} - x_j^{\sim d}\right)/p_{\sim d}\left(x_j^{\sim d}\right)}{\sum_{j=1}^{M} K_{\sim d}\left(x_m^{\sim d} - x_j^{d}\right)/p_{\sim d}\left(x_j^{\sim d}\right)} \tag{11}$$

One important note is that the ISK-GSA formulation for total effects in Eq. (11) assumes that the d and $\sim d$ distribution samples are independent from each other. There are many cases where this assumption is not valid, a prime example being after implementing Bayesian calibration using Markov chain Monte Carlo methods. In this scenario, several thousand input-output samples may be made available; however, there exists correlation among the input samples. This is a challenge being addressed by the proposed generalized ISK-GSA framework in the next section; however, first, a demonstration of the ISK-GSA methodology is presented.

2.2.4 Mathematical example using ISK-GSA

To demonstrate the computational benefits of the ISK-GSA methodology against the DL and MCE methods, consider a two-parameter model $y = 2 \times {}_1 + x_2$ where both parameters x_1 and x_2 are considered to be independent Gaussian random variables with zero mean and unit variance. Both the analytical first-order and total effects Sobol' indices are presented in Eqs. (12) and (13), and are shown to be equivalent since there are neither parameter interactions within the model nor statistical correlations.

$$S_{x_1,1} = S_{x_1,T} = \frac{Var_{x_1}\{E_{x_2}[y|x_1]\}}{Var(y)} = \frac{4\sigma_{x1}^2}{4\sigma_{x1}^2 + \sigma_{x2}^2} \tag{12}$$

$$S_{x_2,1} = S_{x_2,T} = \frac{Var_{x_2}\{E_{x_1}[y|x_2]\}}{Var(y)} = \frac{\sigma_2^2}{c^2\sigma_1^2 + \sigma_2^2} \tag{13}$$

Using Eqs. (12) and (13) and $\sigma_{x1} = \sigma_{x2} = 1$, the true first-order and total effects indices of x_1 and x_2 are 0.8 and 0.2, respectively. Figure 1 compares sensitivity estimates from N iterations of sensitivities from three methods: the double-loop (DL) method, Saltelli's matrix column exchange method (MCE), and the ISK-GSA method. Latin hypercube sampling (LHS) was used to randomly sample the 2-D input space for $N = 1$ to 400 sensitivity iterations. Note that even though each method undergoes one sensitivity iteration (i.e., getting one estimate of the conditional expectation or variance), the number of model evaluations required for N sensitivity iterations shown in the legend significantly differs. Furthermore, while Fig. 1 is only showing the first-order effects, the legend in Fig. 1 is indicating that the number of model evaluations needed to compute the first-order and total effects indices for the ISK-GSA method at each sensitivity iteration N is $O(N)$ compared to $O(2DN^2))$ and $O((2+2D)N)$ for the DL and MCE methods, respectively.

The results demonstrate that the ISK-GSA method requires less than 1% of the model evaluations required for DL sensitivity estimates and less than 17% compared to the MCE method. Furthermore, the ISK-GSA methodology can update the sensitivity estimate after each model evaluation, meaning

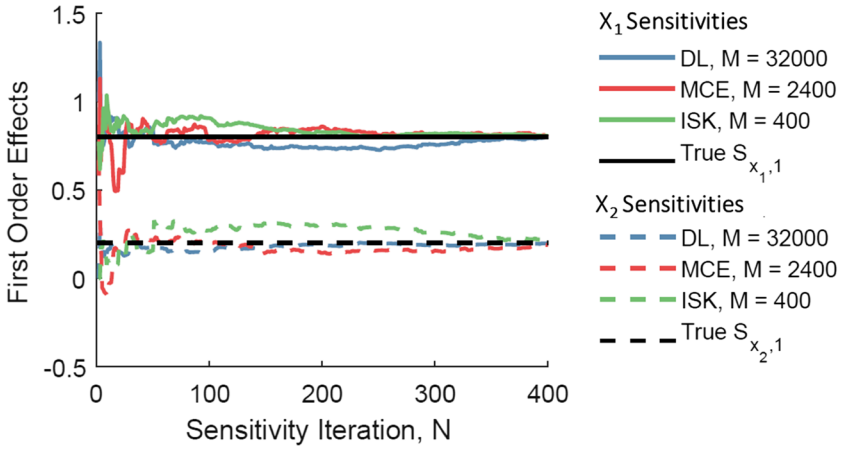

Fig. 1 First-order effects of x_1 (top) and x_2 (bottom) across N sensitivity iterations

the convergence of the sensitivity estimates may be monitored with each successive evaluation of the model. This example will be used further to demonstrate improved convergence properties when the ISK-GSA methodology employs quasi-random number generators as opposed to LHS.

3 Proposed GSA methodology

3.1 Sensitivity analysis with independent variables using ISK-GSA and quasi- random number generators

Quasi-random and pseudo-random number generators are two distinct classes of algorithms used to generate random Monte Carlo samples for numerical integration, uncertainty propagation, and sensitivity analysis. Typical random number-generating algorithms are not truly random but pseudo-random (Knuth 1981) which are the most random-like. For example, the result of a Latin hypercube sampling strategy in two dimensions is shown in the left-hand side of Fig. 2. However, pseudo-random sampling strategies often result in regions of high and low density that can prolong convergence of integrations. Quasi-random sequences (e.g., Sobol' sequences (Sobol 1990), Halton sequences (Halton 1964), or Hammersley sets (Hammersley and Handscomb 1965)) were developed for even coverage over even high-dimensional integral domains and are guaranteed to cover the domain of interest evenly which results in improved efficiency in numerical integration schemes (Sobol 1990).

The proposed methodology uses the Sobol' sequence to fill the input space sequentially after each iteration $n = 1$ to N where the difference in the domain coverage between $(n\text{-}1)^{\text{th}}$ and n^{th} iterations is low. Again considering the model $y = 2 \times {}_1 + x_2$ from section 2.2.4, the advantage of using a Sobol' sequence is evident when N is constrained to a low number of model evaluations ($N = 450$) as shown in Fig. 3. The asymptotic convergence of the sensitivity estimate is observed when a quasi-random Sobol' sequence is used with the ISK-GSA method compared to using a Sobol' sequence with the DL or MCE methods. Thus, a convergence criterion may be applied to terminate the sensitivity analysis and minimize the computational effort. Also, the Sobol' algorithm to sequentially and uniformly fill the space contributes to the "stair-step" pattern of convergence in Fig. 3. In particular, the convergence

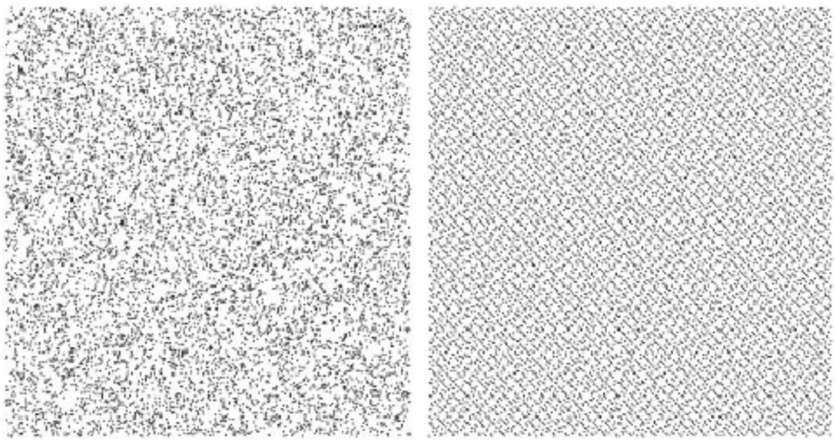

Fig. 2 Latin hypercube design (left) and Sobol' sequence (right) with 10,000 points

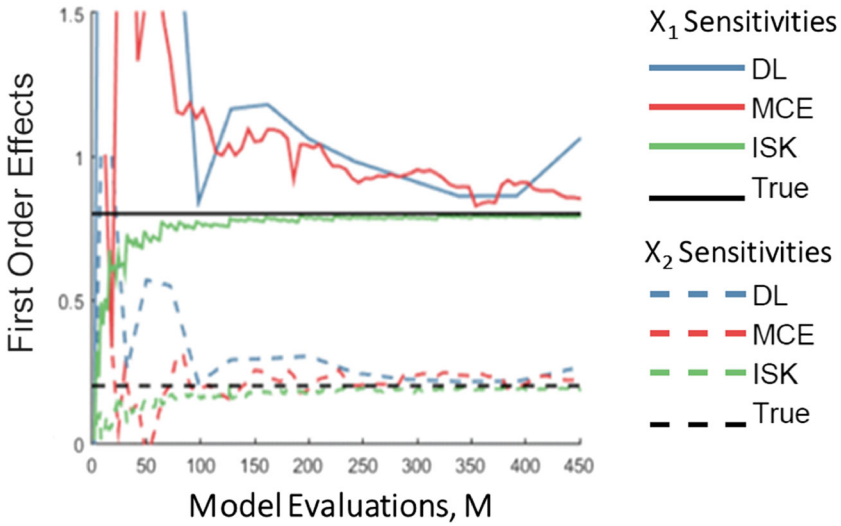

Fig. 3 Comparison of first-order sensitivities using a 2-D Sobol' sequence and LHS design

property is observed using the ISK-GSA method as the number of model evaluations M increases and the kernel bandwidth h_d in each dimension $d = 1,\ldots,D$ decreases according to $h_d = 1.06\sigma_d M^{-1/5}$.

These improvements are especially useful during pre-calibration sensitivity analyses where the analyst is in control of the sampling space and also when the sources of uncertainty are considered independent. As such, the global sensitivity analysis that occurs before calibration will be conducted using the ISK-GSA methodology with Sobol' sequences to reduce the number of simulations required for factor prioritization and dimension reduction. Next, the generalized ISK-GSA is developed to address the challenges of dependent samples in joint posterior parameter distributions.

3.2 Sensitivity analysis with dependent variables using generalized ISK-GSA

Continuing from the development of the ISK-GSA weights in section 2.2.4, the derivation of the kernel regression weights for a generalized ISK-GSA estimate of first-order indices with correlated parameters is presented.

First, as an overview of the probability theory, consider two sets, A and B, that are dependent variables. Their joint distribution $P(\mathrm{A},\mathrm{B})$ is equivalent to the product of a conditional distribution $P(\mathrm{A}|\mathrm{B})$ (or $P(\mathrm{B}|\mathrm{A})$) and a marginal distribution $P(\mathrm{B})$ (or $P(\mathrm{A})$) such that $P(\mathrm{A},\mathrm{B}) = P(\mathrm{B}|\mathrm{A})P(\mathrm{A}) = P(\mathrm{A}|\mathrm{B})P(\mathrm{B})$. Recognizing the relationship between joint, conditional, and marginal distributions in this way leads to modifying the ISK-GSA weight functions in Eqs. (9) and (11) to be able to accommodate dependent inputs.

From the ISK-GSA formulation for first-order Sobol' indices among independent inputs in Eq. (9), it is first recognized that the univariate marginal density $p_d(x^d)$ is equivalent to the joint sampling density $p_{\boldsymbol{D}}(\boldsymbol{x})$ divided by the D-1 multivariate density $p_{\sim d}(\boldsymbol{x}^{\sim d})$. Similarly, the univariate marginal kernel $K_d(x_m^d - x_j^d)$ centered on $\boldsymbol{x}_m^d$ is equivalent to a joint kernel $K_D(\boldsymbol{x}_m^D - \boldsymbol{x}_j^D)$ centered on $\boldsymbol{x}_m^D$ divided by the D-1 dimensional kernel $K_{\sim d}(\boldsymbol{x}_m^{\sim d} - \boldsymbol{x}_j^{\sim d})$ that is centered on $\boldsymbol{x}_m^{\sim d}$. These substitutions of $p_d(x^d)$ and $K_d(x_m^d - x_j^d)$ are made into Eq. (9) to form Eq. (14).

$$w_j^d = \frac{K_D\left(x_m^D - x_j^D\right)p_{\sim d}\left(x_j^{\sim d}\right) \Big/ K_{\sim d}\left(x_m^{\sim d} - x_j^{\sim d}\right)p_D\left(x_j^D\right)}{\sum_{j=1}^{M}\left(K_D\left(x_m^D - x_j^D\right)p_{\sim d}\left(x_j^{\sim d}\right) \Big/ K_{\sim d}\left(x_m^{\sim d} - x_j^{\sim d}\right)p_D\left(x_j^D\right)\right)} \tag{14}$$

Viewing Eq. (14) in terms of two joint distributions divided by marginal distributions, based on probability theory, these ratios are equivalent to conditional distributions in the presence of dependent variables. Therefore, the ratio $K_D(\boldsymbol{x}_m^D - \boldsymbol{x}_j^D)/K_{\sim d}(\boldsymbol{x}_m^{\sim d} - \boldsymbol{x}_j^{\sim d})$ becomes the conditional kernel $K_{d|\sim d}(x^d|\boldsymbol{x}^{\sim d})$ and likewise $p_{\boldsymbol{D}}(\boldsymbol{x})/\, p_{\sim d}(\boldsymbol{x}^{\sim d})$ becomes the conditional distribution $p_{d|\sim d}(x^d|\boldsymbol{x}^{\sim d})$ in Eq. (15).

$$w_j^d = \frac{K_{d|\sim d}\left(x_m^d - x_j^d|X^{\sim d} = x_m^{\sim d}\right) \Big/ p_{d|\sim d}\left(x_j^d|X^{\sim d} = x_m^{\sim d}\right)}{\sum_{j=1}^{M}\left(K_{d|\sim d}\left(x_m^d - x_j^d|X^{\sim d} = x_m^{\sim d}\right) \Big/ p_{d|\sim d}\left(x_j^d|X^{\sim d} = x_m^{\sim d}\right)\right)} \tag{15}$$

With the ISK-GSA kernel regression weight redefined in Eq. (15), the ISK-GSA method is generalized to dependent variables. Note that when there is no dependence between X^d and $\boldsymbol{X}^{\sim d}$, then $p_{d|\sim d}(x^d|\boldsymbol{x}^{\sim d}) = p_d(x^d)$, $K_{d|\sim d}(x^d|\boldsymbol{x}^{\sim d}) = K_d(x^d)$, and Eq. (15) reduces to Eq. (9). Therefore, this is a generalized ISK-GSA formulation. For completeness, the generalized ISK-GSA weights for total effects indices are presented in Eq. (16) and are equivalent to Eq. (11) when X^d and $\boldsymbol{X}^{\sim d}$ are independent.

$$w_j^{\sim d} = \frac{K_{\sim d|d}\left(x_m^{\sim d} - x_j^{\sim d}|X^d = x_m^d\right) \Big/ p_{\sim d|d}\left(x_j^{\sim d}|X^d = x_m^d\right)}{\sum_{j=1}^{M}\left(K_{\sim d|d}\left(x_m^{\sim d} - x_j^{\sim d}|X^d = x_m^d\right) \Big/ p_{\sim d|d}\left(x_j^{\sim d}|X^d = x_m^d\right)\right)} \tag{16}$$

For conceptual understanding, Eqs. (15) and (16) are useful to see the parallels between the generalized ISK-GSA methodology and the independent ISK-GSA formulation from Sparkman et al. However, when computing the generalized ISK-GSA weights, the computations proceed according to Eq. (14) for first-order effects and Eq. (17) for total effects. That is, given the correlated input samples $\boldsymbol{X}_D$, their joint PDF can be estimated and evaluated for each set of inputs $\boldsymbol{x}_j^{\boldsymbol{D}}$. Following, the joint distribution of $\boldsymbol{X}^{\sim d}$ and marginal density of X^d for each dimension are computed from the sample set. In addition, assuming that the joint kernel densities have bandwidths $h_d = 1.06\sigma_d M^{-1/5}$ for each dimension d, the kernels K_D, $K_{\sim d}$, and K_d are fully defined to use in Eqs. (14) and (17).

$$w_j^d = \frac{K_D\left(x_m^D - x_j^D\right) p_{\sim d}\left(x_j^{\sim d}\right) \Big/ K_{\sim d}\left(x_m^{\sim d} - x_j^{\sim d}\right) p_D\left(x_j^D\right)}{\sum_{j=1}^{M}\left(K_D\left(x_m^D - x_j^D\right) p_{\sim d}\left(x_j^{\sim d}\right) \Big/ K_{\sim d}\left(x_m^{\sim d} - x_j^{\sim d}\right) p_D\left(x_j^D\right)\right)} \tag{17}$$

3.3 Time-dependent, multidisciplinary example

The generalized ISK-GSA methodology is demonstrated on a time-dependent, coupled example problem first with independent variables and then with correlated error terms.

Consider the models in Eq. (18) that are representative of multidisciplinary, time-dependent analyses. The models are coupled such (1) the value of model output $y_{1,i}$ moves from 1 toward zero through time as (2) $y_{2,i}$ increases from the initial condition $y_{2,0}$ at a rate of $y_{1,i}$ across time step $\Delta t = 0.1\ s$ until the final time of interest $t_f = 50$ s.

$$\begin{aligned} y_{1,i} &= \frac{y_{2,0}}{y_{2,i-1}} + \varepsilon_1 \\ y_{2,i+1} &= y_{2,i} + y_{1,i}\Delta t + \varepsilon_2 \end{aligned} \tag{18}$$

Three sources of uncertainty—uncertain model errors (ε_1, ε_2) and the initial condition $y_{2,0}$—are considered for GSA analysis and are propagated through the coupled system first as independent Gaussian random variables with statistics shown in Table 1 and then as dependent Gaussian random variables with the correlation structure shown in Eq. (19). A negative correlation between model discrepancy parameters was observed after calibration in refs. DeCarlo et al. 2016 and DeCarlo et al. 2014, with some correlations tending toward negative 1; thus, a negative correlation $\rho = -0.5$ is imposed between model errors ε_1 and ε_2 in Eq. (19).

$$\rho = \begin{bmatrix} 1 & 0 & 0 \\ 0 & 1 & -0.5 \\ 0 & -0.5 & 1 \end{bmatrix} \tag{19}$$

A three-dimensional Sobol' sequence was generated for $y_{2,0}$, ε_1, and ε_2 and propagated through to model outputs y_1 and y_2 for $t_f = 50$ s. Figure 4 demonstrates the prediction uncertainty in both y_1 and y_2 (1) when just the uncertainty in the input condition is propagated as a random variable (RV) with ε_1 and ε_2 fixed at their mean values (black), (2) when all three sources of uncertainty are propagated as independent RVs (blue), and (3) when correlation among ε_1 and ε_2 is considered (green). It is observed in Fig. 4a that a negative correlation between ε_1 and ε_2 slightly increases uncertainty in y_1 predictions compared to the independent case, however, due to the inversely proportional relationship between $y_{1,i}$ and $y_{2,i\text{-}1}$. However, Fig. 4b demonstrates that the error dependence decreases the uncertainty in downstream y_2 predictions from the additive relationship between $y_{2,i}$ and $y_{1,i}$. Note that since ε_1 and ε_2 both have zero mean, the mean predictions overlap for each of the three cases presented in Fig. 4a, b.

Table 1 Uncertain model inputs and errors

Parameter	Mean	Variance
$y_{2,0}$	20	4
ε_1	0	4e−4
ε_2	0	4e−4

The sensitivities throughout time to $y_{2,0}$, ε_1, and ε_2 for each model were computed using the generalized ISK-GSA methodology for both the independent and dependent variable cases. The first-order effects (Eq. (14)) and the total effects Sobol' indices (Eq. (16)) were computed with the three-dimensional Sobol' sequence of $N = 1000$ which were assumed to be the conditional cumulative density function (CDF) values in each dimension d. Note that in the dependent parameter case, an iterative procedure was used to map the conditional CDF values to the parameter space; however, in the independent case, the marginal CDFs were used.

The first-order effects and total effects for model output y_1 from both the independent and dependent variable cases are shown in Fig. 5. First, it is observed in Fig. 5a, b that the first-order and total effects on y_1 are equivalent in the independent parameter case indicating that the parameter interactions within the model itself are insignificant. The sensitivity of y_1 to the initial condition $y_{2,0}$ appears to decrease over time which means that its relative uncertainty contribution to the output is decreasing compared to the growing uncertainty contributions from ε_1 and ε_2. In addition, there is a trade-off between the effects ε_1 and ε_2 through time as the model output y_1 becomes more sensitive to the uncertainty in ε_2 due to model interactions.

In contrast to the independent variable case, Fig. 5c shows that individual first-order effects of both ε_1 and ε_2 change through time when correlation is considered. First, the first-order effects of ε_1 immediately decrease at $t = 0$ s due to the correlation of -0.5 with ε_2. Then, the first-order effects of ε_2 do not approach 1 as in the independent case, but rather approach approximately 0.65. However, y_1 sensitivity to $y_{2,0}$ in

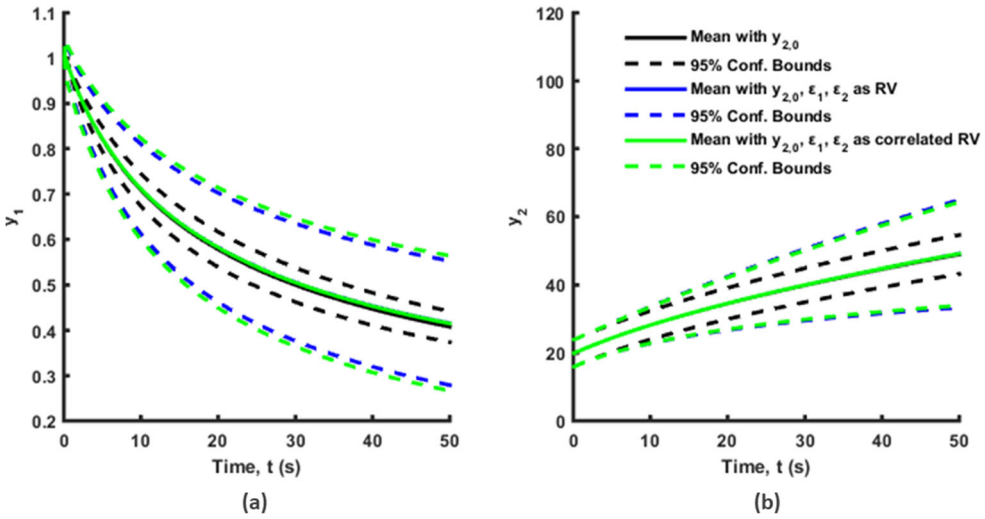

Fig. 4 Coupled y_1 predictions (**a**) and y_2 predictions (**b**) through $t_f = 50$ s

Fig. 5c undergoes little change between the independent and dependent cases since $y_{2,0}$ itself is not correlated with any other parameter. For the dependent variable case in Fig. 5d, however, the total effects of ε_2 immediately increase from 0 to 0.35 at $t = 0$ s due to the correlation with ε_1 and it is ε_1 that approaches approximately 0.35 as opposed to 0 in the independent case. This is intuitive since the total effects Sobol' index captures parameter interactions regardless if they are intrinsic to the model or the parameters themselves. Note that these ISK-GSA estimates maintain the summation criteria of $\Sigma S_{d,1} \leq 1$ and $\Sigma S_{d,T} \geq 1$ of the first-order and total effects, respectively, over all time instants.

The first-order and total effects sensitivity indices for the y_2 prediction are shown in Fig. 6 with similar conclusions drawn from the sensitivities of y_1 from Fig. 5. First, the first-order sensitivities in Fig. 6 and total effects indices in Fig. 6b are equivalent in the independent case due to negligible parameter interactions within the model. Second, y_2 sensitivity to $y_{2,0}$

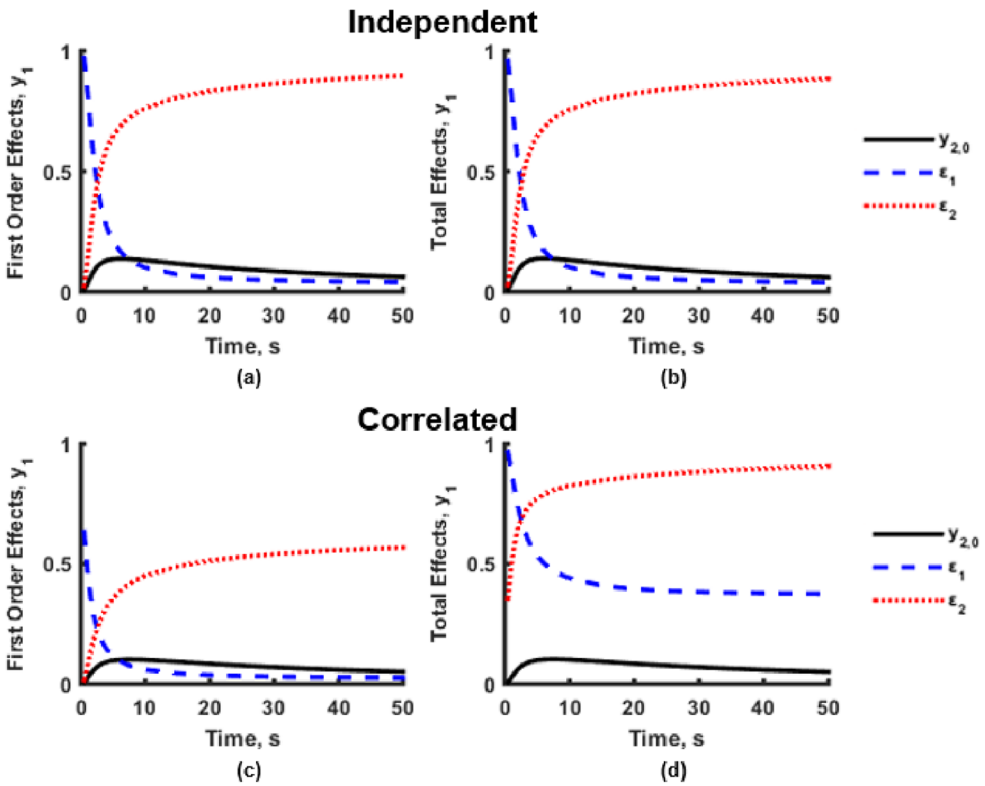

Fig. 5 First-order and total effects on model output y_1 with independent (top) and dependent (bottom) variables

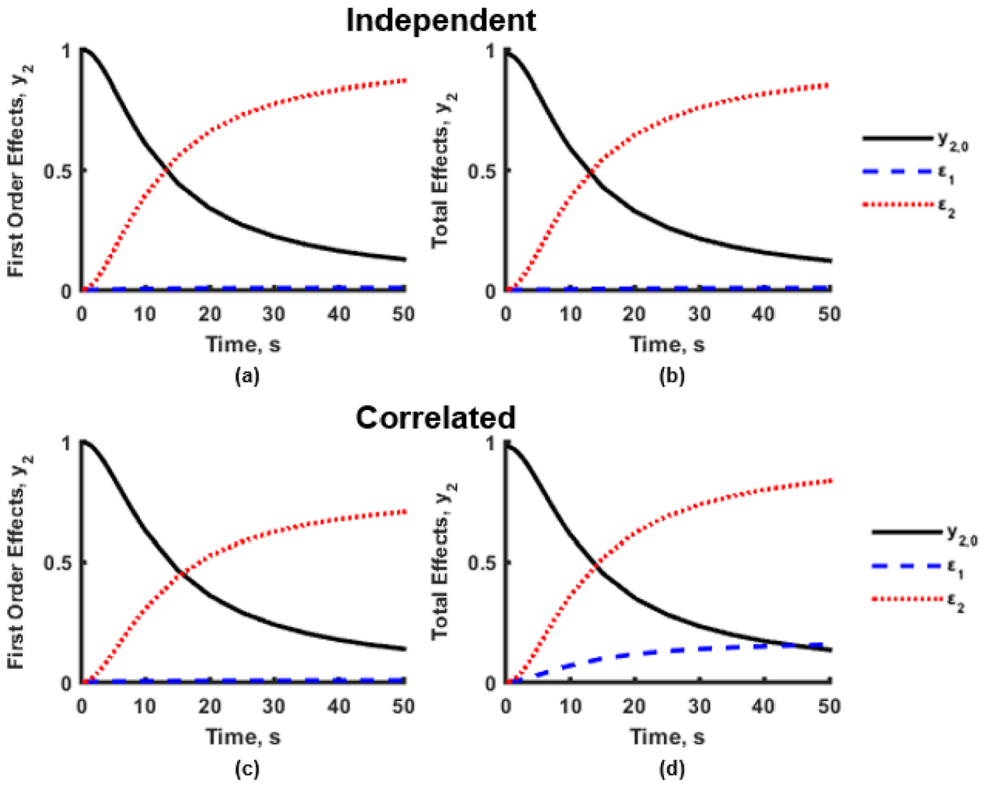

Fig. 6 First-order and total effects on model output y_2 with independent (**a**, **b**) and dependent (**c**, **d**) parameters

undergoes little change between the independent and dependent variable cases since $y_{2,0}$ itself is not correlated with any other parameter.

For the dependent variable cases in Fig. 6c, d, it is observed that the first-order effects of y_2 in Fig. 6c sum is close to unity since the sensitivity of y_2 to ε_1 is low; however, in Fig. 6d, the total effects sensitivities of y_2 to both ε_1 and ε_2 increase over time due to the effect of correlation between ε_1 and ε_2.

Figure 7a, b illustrates differences between positive and negative correlations on the first-order and total effects sensitivities of both model outputs to error parameter ε_2 through time. First, it is observed that as the correlation increases from -0.5 to -0.9, the first-order effects of ε_2 on y_1 become closer to 0. It can be shown further that as the correlation approaches -1, the first-order effects of both ε_1 and ε_2 approach 0, whereas the total effects in Fig. 7b approach 1.

However, when the correlation between the parameters is positive, it is observed in Fig. 7a, b that the first-order effects of ε_2 on y_1 are greater than the total effects. Again, this is attributed to the inversely proportional relationship between $y_{1,i}$ and $y_{2,i\text{-}1}$ (and, by extension, ε_2), and this phenomenon does not occur in the first-order and total effects of ε_2 on model output y_2 in Fig. 7c, d. In both positive and negative correlation cases in Fig. 7c, d, the first-order effects of ε_2 on model output y_2 decreased compared to the independent ($\rho = 0$) case, with the positive correlation cases exhibiting lower first-order effects over time and higher total effects than the negative correlation cases. It is interesting to note that the independent case in Fig. 7c represents the maximum first-order effect; however, the $\rho = 0$ case does not bound the total effects sensitivities in Fig. 7d. In general, the same is true between the first-order and total effects on y_1 in Fig. 7a, b; however, the relationship between the positive and negative correlations with the independent case in the total effects is opposite, with the positive correlations having lower total effects than the independent case for y_1 but higher total effects for y_2.

3.4 Computational effort and dimension considerations

For the three-parameter example, the sensitivity convergence rates between the independent and correlated cases were equal using the generalized ISK-GSA methodology with Sobol' sequences, meaning that the extension of the ISK-GSA methodology to dependent variables does not incur added computational cost. However, the generalized ISK-GSA methodology, like many kernel-based methods, does lose efficiency as the dimension of the input increases.

As an example of the efficiency from the proposed method with increasing dimension, the first-order indices of both y_1 and y_2 in the example on average converged in 250 iterations using 1-D Sobol' sequences. In contrast, the total effects indices converged in approximately 800 iterations from Sobol' sequences in two dimensions. One adaptation may be variable bandwidth kernels (Terrell and Scott 1992) where a cross-

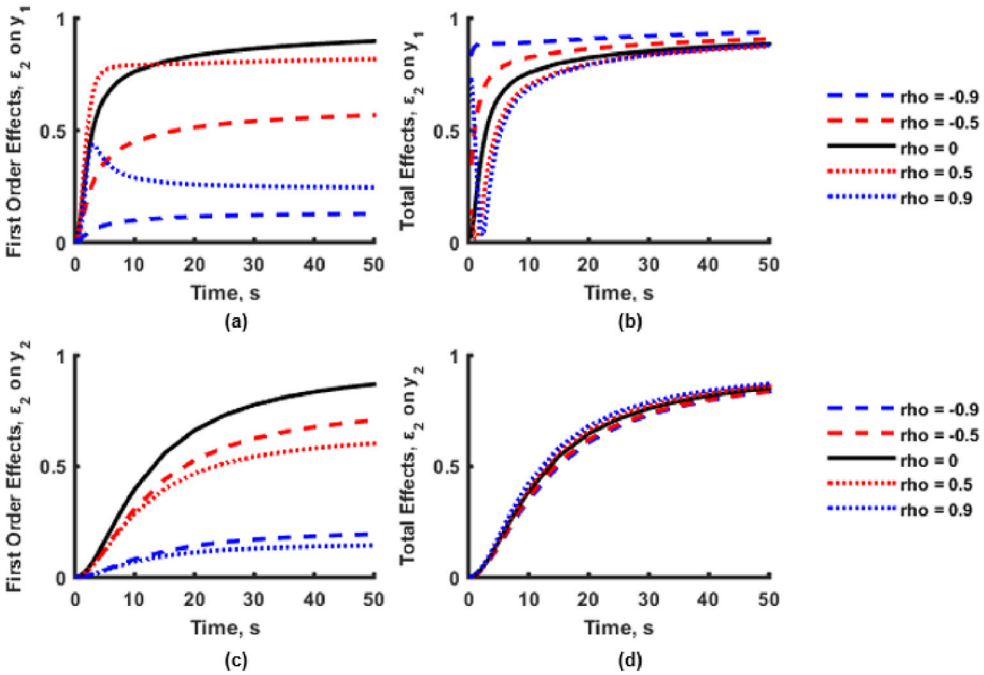

Fig. 7 Effect of ε_1 and ε_2 correlation on the sensitivities of y_1 to ε_2 (**a**, **b**) and y_2 to ε_2 (**c**, **d**)

validation step is employed after each iteration to select the optimum bandwidth rather than using the empirical rule of thumb. Also, a less stringent stopping criterion may be imposed as the dimension of problem increases; however, this is only viable when Sobol' sequences are used in conjunction with the ISK-GSA methodology for which asymptotic convergences of the sensitivity estimates are observed.

4 Application example: coupled aerothermal sensitivities

4.1 Calibrated aerothermal models

The US Air Force (USAF) has identified the need for reusable high-speed aircraft that can endure the combined aerodynamic, thermal, and acoustic loads observed in hypersonic flight environments (Rose 2008). Due to limited operational data and the inability to fully reproduce hypersonic loads in ground facilities, there is significant uncertainty surrounding the structural response and material degradation of an aircraft structure that is repeatedly subjected to significant, fluctuating aeropressures and high thermal gradients from high Mach flights (West and Hosder 2015). As a result, the highly coupled aerothermoelastic response of a structure characterized by fluid-thermal-structural interactions (FTSI) is studied primarily via single- and partial-physics constituent models (e.g., aero-elastic, fluid-thermal, heat transfer, aero-acoustic) (Bodony et al. 2010; Culler and McNamara 2011a).

Partitioned aerothermal-structural coupling strategies have been pursued to simulate and study FTSI in the absence of full-scale physical tests under fully representative hypersonic loads (Kontinos 1997; Blevins et al. 2009; Culler and McNamara 2011b; Falkiewicz and Cesnik 2011). At high Mach numbers, fluid-structural coupling between aerodynamic pressure (p_{surface}) and a deforming structure (w) is accompanied by significant aerodynamic heat loads (Q_{aero}) from large temperature gradients within the fluid boundary layer (Anderson 2006). These aerodynamic heat loads transfer through the structure, augment the temperature-dependent material properties, and lead to non-uniform thermal gradients ($T_{\text{structure}}$) which cause further deformation into the flow. In addition, a significant modeling uncertainty exists due to the limited ability perform ground tests and confidently predict the structural reliability, risk, and performance of these aircraft (Liguore and Tzong 2011), and coupled interactions between multidisciplinary models introduce additional uncertainty during the long duration simulation.

A Bayesian model calibration was performed on the aerothermal subset of an aerothermoelastic analysis which is shown in Fig. 8. Aerodynamic heat flux Q_4 ("location 4" indicating a point of interest along the panel) is predicted by Eckert's reference temperature method (Eckert 1956) which is a semi-empirical method used to approximate convective heating of aerospace vehicles traveling between Mach 1.4 and 15. The Eckert's reference temperature (ERT) method prediction uses boundary layer relations from incompressible

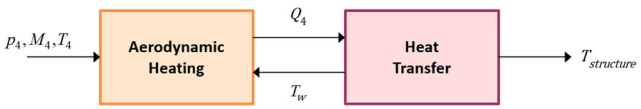

Fig. 8 Aerothermal coupling

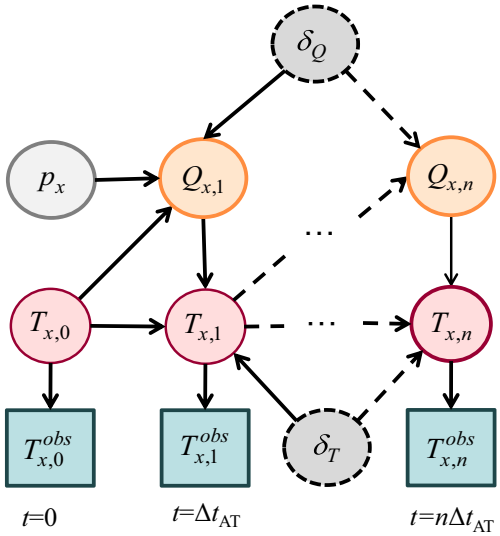

Fig. 9 Dynamic Bayesian network for the calibration of coupled aerothermal models

flow theory with flow properties evaluated at a reference condition (i.e., the reference temperature). The ERT model is then coupled with the 1-D heat equation to predict evolution of the structural temperatures $T_{\text{structure}}$ and wall temperatures T_{w} of a panel upstream of an oblique shock.

For simplicity, the notation T_n indicates the wall temperature at time n at a given x location, and the aerothermal analysis iterates between heat flux Q_n and wall temperature T_n predictions through n aerothermal time steps at a rate of Δt_{AT}. Assuming a calorically perfect gas (Eckert 1956), Eckert's reference temperature T_n^* at time step n is computed using Eq. (20) where T_n^{aw} and T_n represent the adiabatic wall and current wall temperature, respectively, and T_n^{bl} and T_n^e are the boundary layer temperature and temperature at the leading edge of the panel ($x = 0$). Eckert's reference temperature method predicts the applied heat flux Q_{n+1}at time step $n + 1$ using the Stanton number St_n^* (a dimensionless number that relates the heat transferred to the heat capacity of the fluid), the reference flow density ρ_n^*, and the reference specific heat $C_{p,n}^*$ along with the inviscid flow velocity U_n based on the reference temperature as shown in Eq. (21).

$$T_n^* = T_n^e + 0.5\left(T_n - T_n^{bl}\right) + 0.22\left(T_n^{aw} - T_n^e\right) \tag{20}$$

$$Q_{n+1} = St_n^* \rho_n^* U_n C_{p,n}^* \left(T_n^{aw} - T_n\right) \tag{21}$$

The wall temperature T_{n+1} at the $(n+1)^{\text{th}}$ time step is predicted with 1-D heat transfer using the current heat flux Q_{n+1} and wall temperature T_n predicted from the previous time step. The 1-D heat transfer equation shown in Eq. (22) is applicable to the thin-walled spherical dome experiments performed by Glass and Hunt (1986) that are used for calibration and detailed in the next section. Assuming a uniform initial wall temperature $T_0 = 300$ K at $t = 0$, Eqs. (20)–(22) are solved explicitly at each aerothermal time step of $\Delta t_{AT} = 0.05$ s.

$$T_{n+1} = T_n + \frac{Q_{n+1}(T_n)\Delta t_{AT}}{\rho_{\text{dome}} C_{p,\text{dome}} \tau_{\text{dome}}} \tag{22}$$

Based on aerothermal tests conducted in the NASA Langley HTT tunnel (Glass and Hunt 1986), the reported heat flux measurements were used to reconstruct a 3-s temperature history at a rate of $\Delta t = 0.05$ s (20 samples per second). Measurement noise was assumed to be zero mean Gaussian with a standard deviation of 1 K. Using this source of time-dependent temperature data to calibrate the aerothermal models, Fig. 9 depicts a dynamic Bayesian network when two sources of model discrepancy—δ_Q and δ_T—are propagated through the network at each time step.

Bayes' formula for the aerothermal model calibration with the time-dependent temperature data is shown in Eq. (23), where the joint posterior distribution of the model discrepancies δ_Q and δ_T is desired after observing data $\boldsymbol{T}^{\text{obs}}$. The data

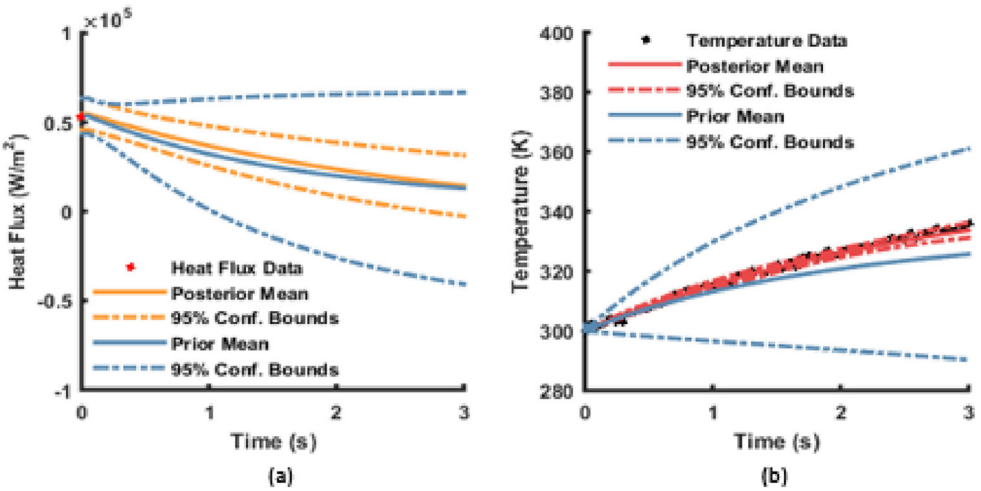

Fig. 10 Prior and posterior heat flux (**a**) and temperature (**b**) predictions

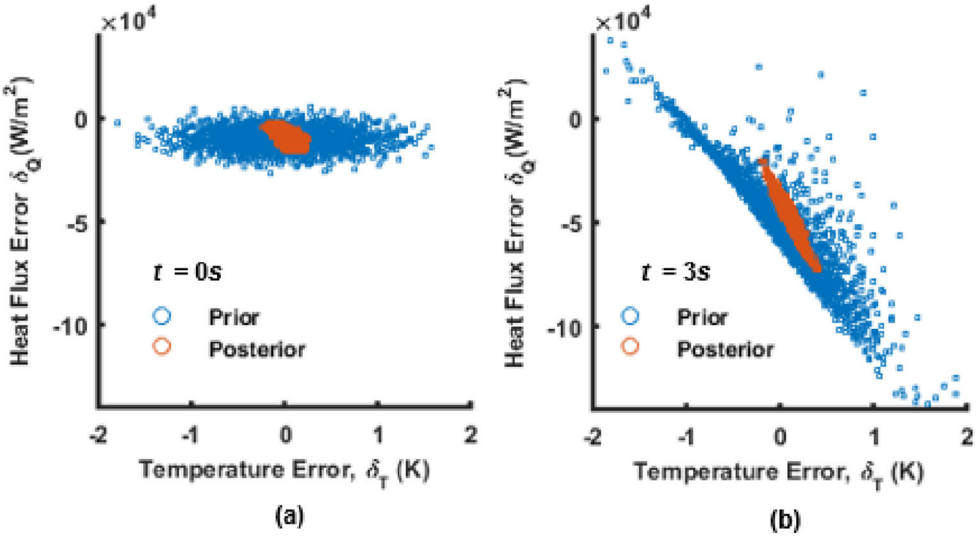

Fig. 11 Joint prior and posterior distributions for δ_Q and δ_T at $t =$ 0 s (**a**) and $t = 3$ s (**b**)

interval Δt_{obs} and aerothermal prediction interval Δt_{AT} need not be equivalent as shown in Fig. 9 but were chosen as such for the calibration herein.

$$\pi\left(\delta_T, \delta_Q | T^{\text{obs}}_{1,\ldots,n}\right) = \frac{\pi\left(T^{\text{obs}}_{1,\ldots,n} | \delta_T, \delta_Q\right)\pi(\delta_T, \delta_Q)}{\int L(\delta_T, \delta_Q)\pi(\theta_m, \theta_\delta)\partial\delta_T\partial\delta_Q} \propto L(\delta_T, \delta_Q)\pi(\delta_T, \delta_Q) \tag{23}$$

Note that the aerodynamic heating errors δ_Q and heat transfer errors δ_T propagate through each iteration and are functions of the changing model inputs according to Eqs. (24) and (25).

$$\delta_Q(T_{n-1}) = c_0 + c_1 \frac{T_{n-1} - T_0}{T_4} \tag{24}$$

$$\delta_T(Q_n) = (d_0 + d_1 Q_n)\Delta t \tag{25}$$

Thus, the four calibration parameters were the model error parameters $\boldsymbol{\theta} = [c_0, c_1, d_0, d_1]$. The prior distributions among the parameters $\boldsymbol{\theta}$ were independent, and thus the generalized ISK-GSA methodology with Sobol' sequences was performed to down-select among the independent calibration parameters for possible calibration dimension reduction; however, all parameters were deemed significant (total effects indices > 0.05). Thus, the calibration with all four parameters was performed using 10^3 slice samples (Neal 2003) and the prior and posterior heat flux and temperature predictions with 95% confidence bounds are shown in Fig. 10a, b, respectively, where the post-calibration prediction confidence in temperature increased across all time steps by reducing uncertainty in both Eckert's reference temperature and 1-D heat transfer predictions.

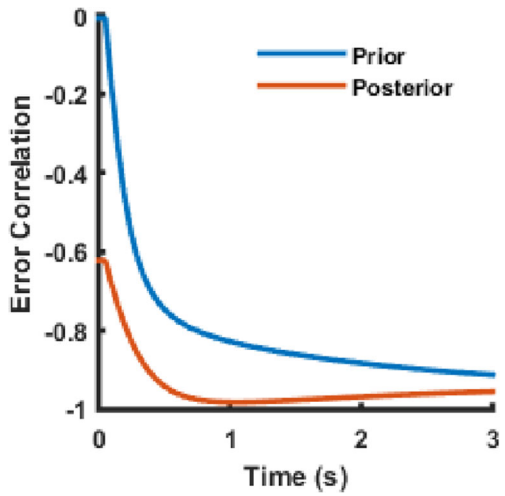

Fig. 12 Prior and posterior correlation between δ_Q and δ_T

The posterior correlation among the four discrepancy parameters is shown in Eq. (26) and provides one application for the generalized ISK-GSA methodology for dependent variables. In addition, both the prior and posterior model discrepancy distributions of δ_Q and δ_T are correlated as well, and it is in this space that we apply the generalized ISK-GSA methodology to the coupled, aerothermal analysis. The prior and posterior correlations among the model discrepancy terms δ_Q and δ_T are depicted in Fig. 11a, b first at the beginning of the analysis at $t_0 = 0$ s and then at the end at $t_f = 3$ s.

$$\rho_\theta = \begin{bmatrix} 1 & -0.29 & -0.42 & 0.02 \\ -0.29 & 1 & -0.54 & 0.10 \\ -0.42 & -0.54 & 1 & -0.59 \\ 0.02 & 0.10 & -0.59 & 1 \end{bmatrix} \tag{26}$$

At $t = 0$ s in Fig. 11a, correlation ρ_δ between model discrepancies is observed to be − 0.6 among the posterior samples, whereas $\rho_\delta = 0$ among the prior model discrepancy predictions since the discrepancy parameters $\boldsymbol{\theta}$ were independent before calibration. However, strong negative correlations are present in both prior model discrepancy predictions at $t = 3$ s in Fig. 11b. First, Fig. 11b shows the prior correlation between δ_Q and δ_T becomes − 0.9 solely due to discrepancy

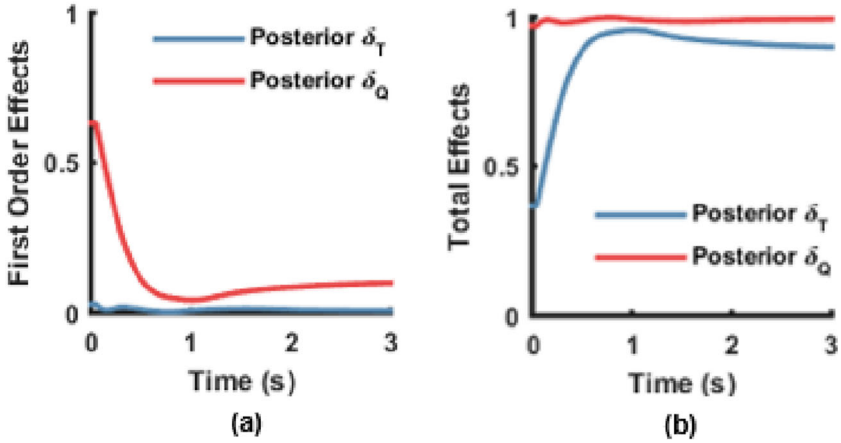

Fig. 13 Posterior heat flux sensitivities to δ_Q and δ_T through time

interactions that are inherent to the prediction. In comparison, the posterior correlation between δ_Q and δ_T changes from -0.6 at $t = 0$ s and grows to -0.95 at $t = 3$ s in Fig. 11b from model interactions through time. The trend of both the prior and posterior model error correlations through time in Fig. 12 demonstrates that the input parameter correlations affect the coupled prediction until the coupling effects become more prominent over time, and extending the analysis through demonstrates the convergence of both prior and posterior error correlations to -0.9.

Note that the generalized ISK-GSA methodology is also needed to compute the prior sensitivities of the model outputs to δ_Q and δ_T through time as well, since the errors become correlated through time due to the model interactions. The difference, however, lies in how the input-output samples are generated, where prior sensitivity analysis uses 4-D Sobol' sequence and the posterior analysis uses samples generated from the Markov chain Monte Carlo (MCMC) algorithm. Therefore, the posterior sensitivities of the coupled heat flux and temperature predictions to model discrepancies δ_Q and δ_T are computed using the existing input-output samples from calibration and the generalized ISK-GSA methodology.

4.2 Post-calibration aerothermal sensitivities with the generalized ISK-GSA methodology

The post-calibration sensitivity analysis for the aerothermal example was performed using the last 4×10^3 posterior samples from the 10^4 slice samples generated from calibration to reduce the computational effort required to compute the ISK-GSA results at each time instant. The posterior heat flux sensitivities through time in Fig. 13 demonstrate that the negative correlation between δ_Q and δ_T at all time instants first decreases the first-order effect sensitivities of δ_Q from 1 (observed in the prior case) to 0.6, which corresponds to the negative posterior discrepancy correlation of -0.6 seen at $t = 0$ s in Fig. 12. Then, the posterior sensitivity of Q_n to model discrepancy δ_Q follows a similar trend to the posterior discrepancy correlation in Fig. 12. This is because a correlation close to -1 indicates strong interactive effects, which in turn reduce the first-order effects of the variable. Similarly, the posterior total effects of δ_T on heat flux have increased to 0.4 at $t = 0$ s due to the correlation with δ_Q, approach 1, and then asymptotically approach approximately 0.85, which can be considered as the total effects sensitivity from interactions inherent to the model.

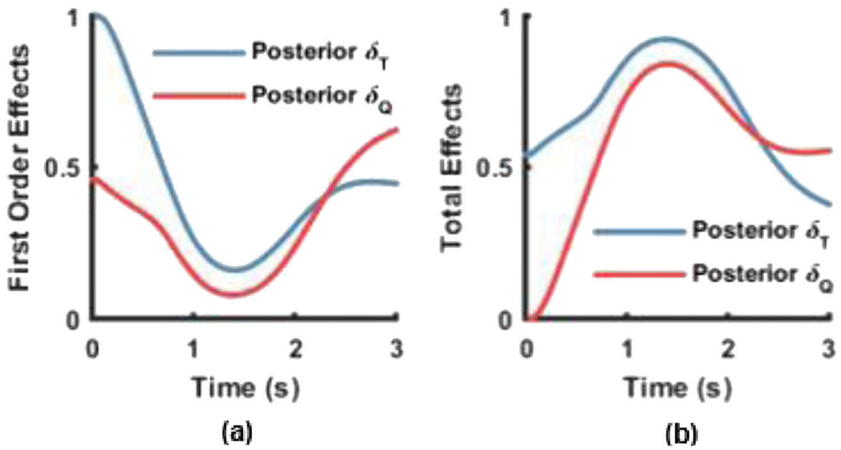

Fig. 14 Posterior temperature sensitivities to δ_Q and δ_T through time

The posterior sensitivities of the predicted temperature to the model discrepancies δ_Q and δ_T through time are shown in Fig. 14. First, in contrast to the heat flux sensitivities in Fig. 13, the first-order effects in Fig. 14a indicate influence from a source of positive correlation because, rather than the first-order effects of δ_T decreasing from treating the correlation as interactions, the first-order effects of δ_Q increase and the first-order effects sum to greater than 1 at $t = 0$ s. Further, the total effects in Fig. 14a sum to less than 1, and in this case, temperature sensitivities to δ_T decrease. This prompts further investigation into the relationships between temperature T and δ_Q and δ_T through time and the effect of positive correlations on GSA sensitivity indices of coupled model outputs through time.

5 Summary and future work

Global sensitivity analysis computations for independent variables were improved first by pairing quasi-random number generators with the ISK-GSA methodology. Furthermore, efficient GSA computations were extended to correlated variables by generalizing the ISK-GSA method and applying it to coupled models interacting through time and then to existing posterior input-output samples from Bayesian calibration. A summary of conclusions drawn from this research are as follows:

1. When paired with quasi-random sequences, the ISK-GSA sensitivity estimate asymptotically converges to the true sensitivity. Therefore, a sensitivity convergence criterion can be used to minimize the number of model evaluations needed for global sensitivity analysis among independent variables (e.g., before calibration).
2. The generalized ISK-GSA methodology for dependent variables improved the efficiency of GSA for the following:
   (a) coupled model predictions, where parameter interactions within the models become more prominent over time; and
   (b) post-calibration sensitivity analyses by allowing the direct use of correlated posterior samples obtained from calibration.
3. The effects of both positive and negative correlations on both the first-order and total effects were demonstrated. For the simplified time-dependent example, negative correlations between model errors maintained the expected summation criteria for first-order and total effects; however, positive correlations did not. Similar results were observed for the aerothermal problem, and thus, the effects of positive correlations on the sensitivities of coupled models require further understanding.
4. The generalized ISK-GSA method led to a broader analysis of sensitivity in coupled, time-dependent analyses where first-order and total effects are influenced by both parameter correlation and model interactions through time. For example, in the aerothermal application example, correlation effects on the sensitivity estimates were seen in early time instances until coupling effects became more significant through time.

In future work, this methodology may be embedded directly into MCMC sampling procedures to monitor the evolution of the posterior parameters after each sample. In this way, sources of uncertainty can be down-selected adaptively as the likelihood is explored in the MCMC algorithm. This may also account for the possibility that some regions of the likelihood may be more sensitive to a subset of the parameter space than other regions. Also, at a given point in the calibration, the generalized ISK-GSA sensitivity result may indicate convergence globally or within the local likelihood region, which may inform the optimal step-sizes taken in each dimension and further improve calibration convergence.

Acknowledgments The authors gratefully acknowledge Dr. Daniel Sparkman for valuable discussions on the fundamentals of the ISK-GSA methodology which provided the basis for the methodology herein.

Funding information This research is sponsored by the National Defense Science and Engineering Graduate (NDSEG) fellowship and approved for public release case 88ABW-2017-3778 cleared 02 Aug 2017.

References

Anderson JD Jr (2006) Hypersonic and high-temperature gas dynamics, 2nd edn. American Institute of Aeronautics and Astronautics, Reston, VA

Blevins RD, Bofilios D, Holehouse I, et al (2009) Thermo-vibro-acoustic loads and fatigue of hypersonic flight vehicle structure. AFRL-RB-WP-TR-2009-3139

Bodony DJ, Zagaris G, Reichert A, Zhang Q (2010) Reprint of: Aeroacoustic predictions in complex geometries. Procedia IUTAM 1:234–243. https://doi.org/10.1016/j.piutam.2010.10.025

Camberos J, Josyula E, Lambe L (2007) Quasi-random Monte Carlo integration for computing dissociation rates. In: 39th AIAA Thermophysics conference. AIAA 2007–4260

Cukier RI, Fortuin CM, Schuler KE et al (1973) Study of the sensitivity of coupled reaction systems to uncertainties in rate coefficients. J Chem Phys 59:3873–3878. https://doi.org/10.1063/1.1680571

Culler AJ, McNamara JJ (2011a) Impact of fluid-thermal-structural coupling on response prediction of hypersonic skin panels. AIAA J 49: 2393–2406. https://doi.org/10.2514/1.J050617

Culler AJ, McNamara JJ (2011b) Fluid-thermal-structural modeling and analysis of hypersonic structures under combined loading. In: 52nd

AIAA/ASME/ASCE/AHS/ASC Structures, Structural Dynamics, and Materials Conference. AIAA 2011–1965. Denver, **CO**

DeCarlo EC, Mahadevan S, Smarslok BP (2013) Bayesian calibration of aerothermal models for hypersonic air vehicles. In: 54th AIAA/ASME/ASCE/AHS/ASC Structures, Structural Dynamics, and Materials and Co-located Conferences. AIAA 2013–1683. Boston, MA

DeCarlo EC, Mahadevan S, Smarslok BP (2014) Bayesian calibration of coupled aerothermal models using time-dependent data. In: 16th AIAA non-deterministic approaches conference at AIAA SciTech. AIAA 2014–0123. National Harbor, MD

DeCarlo EC, Smarslok BP, Mahadevan S (2016) Segmented Bayesian calibration of multidisciplinary models. AIAA J 54:3727–3741. https://doi.org/10.2514/1.J054960

Eckert ERG (1956) Engineering relations for heat transfer and friction in high velocity laminar and turbulent boundary layer flow over surfaces with constant pressure and temperature. Trans ASME 78: 1273–1283

Falkiewicz N, Cesnik CE (2011) Enhanced modal solutions for structural dynamics in aerothermoelastic analysis. In: 52nd AIAA/ASME/ASCE/AHS/ASC Structures, Structural Dynamics & Materials Conference. AIAA 2011–1963. Denver, CO

Gamboa F, Janon A, Klein T et al (2016) Statistical inference for Sobol pick-freeze Monte Carlo method. Statistics (Ber) 50:881–902. https://doi.org/10.1080/02331888.2015.1105803

Glass CE, Hunt LR (1986) Aerothermal tests of spherical dome protuberances on a flat plate at a Mach number of 6.5. NASA-TP-2631

Haldar A, Mahadevan S (2000) Probability, reliability and statistical methods in engineering design. Wiley, New York

Halton JH (1964) Algorithm 247: radical-inverse quasi-random point sequence. Commun ACM 7:701–702. https://doi.org/10.1145/355588.365104

Hammersley JM, Handscomb DC (1964) Monte Carlo methods. In: Monographs on statistics and applied probability. Methuen & Co, London

Hastings WK (1970) Monte Carlo sampling methods using Markov chains and their applications. Biometrika 57:97–109

Hu Z, Du X (2013) Time-dependent reliability analysis with joint upcrossing rates. Struct Multidiscip Optim 48:893–907. https://doi.org/10.1007/s00158-013-0937-2

Hu Z, Mahadevan S (2015) Time-dependent system reliability analysis using random field discretization. J Mech Des 137:101404. https://doi.org/10.1115/1.4031337

Hu Z, Mahadevan S (2016) Global sensitivity analysis-enhanced surrogate (GSAS) modeling for reliability analysis. Struct Multidiscip Optim 53:501–521. https://doi.org/10.1007/s00158-015-1347-4

Jia G, Taflanidis AA (2016) Efficient evaluation of Sobol' indices utilizing samples from an auxiliary probability density function. J Eng Mech 142:4016012. https://doi.org/10.1061/(ASCE)EM.1943-7889.0001061

Knuth DE (1981) The art of computer programming, 2nd edn. Addison-Wesley Publishing cmpany, Reading, Massachusetts

Kontinos D (1997) Coupled thermal analysis method with application to metallic thermal protection panels. J Thermophys Heat Transf 11: 173–181. https://doi.org/10.2514/2.6249

Kostanjčar Z, Jeren B, Cerovec J (2009) Particle filters in decision making problems under uncertainty. Automatika 50:245–251

Kucherenko S, Tarantola S, Annoni P (2012) Estimation of global sensitivity indices for models with dependent variables. Comput Phys Commun 183:937–946

Li C, Mahadevan S (2016) An efficient modularized sample-based method to estimate the first-order Sobol′ index. Reliab Eng Syst Saf 153: 110–121. https://doi.org/10.1016/j.ress.2016.04.012

Liang C, Mahadevan S (2015) Bayesian sensitivity analysis and uncertainty integration for robust optimization. J Aerosp Inf Syst 12:189–203. https://doi.org/10.2514/1.I010268

Liang C, Mahadevan S (2016) Multidisciplinary optimization under uncertainty using Bayesian network. SAE Int J Mater Manf 9:419–429. https://doi.org/10.4271/2016-01-0304

Liang C, Mahadevan S, Sankararaman S (2015) Stochastic multidisciplinary analysis under epistemic uncertainty. J Mech Des 137: 021404. https://doi.org/10.1115/1.4029221

Liguore SL, Tzong G (2011) Identification of knowledge gaps in the predictive capability for response and life prediction of hypersonic vehicle structures. In: 52nd AIAA/ASME/AHS/ASC Structures, Structural Dynamics and Materials Conference. AIAA 2011–1961. Denver, CO, pp 1–9

Mahadevan S, Liang B (2011) Error and uncertainty quantification and sensitivity analysis in mechanics computational models. Int J Uncertain Quantif 1:147–161. https://doi.org/10.1615/IntJUncertaintyQuantification.v1.i2.30

Mara TA, Tarantola S (2012) Variance-based sensitivity indices for models with dependent inputs. Reliab Eng Syst Saf 107:115–121

Neal RM (2003) Slice sampling. Ann Stat 31:705–767. https://doi.org/10.1214/aos/1056562461

Ratto M, Pagano A, Young P (2007) State dependent parameter metamodelling and sensitivity analysis. Comput Phys Commun 177:863–876. https://doi.org/10.1016/j.cpc.2007.07.011

Rose LJ (2008) Air Force research laboratory's focused long term challenges. In: Proceedings of SPIE 6981, Defense Transformation and Net-Centric Systems. 698103

Saltelli A, Annoni P, Azzini I et al (2010) Variance based sensitivity analysis of model output. Design and estimator for the total sensitivity index. Comput Phys Commun 181:259–270. https://doi.org/10.1016/j.cpc.2009.09.018

Saltelli A, Ratto M, Andres T, et al (2008) Global sensitivity analysis. The Primer, 1st edn. John Wiley & Sons, Ltd, Hoboken, NJ

Sankararaman S (2012) Uncertainty quantification and integration in engineering systems. Dissertation, Vanderbilt University

Smarslok B, Culler A, Mahadevan S (2012) Error quantification and confidence assessment of aerothermal model predictions for hypersonic aircraft. In: 53rd AIAA/ASME/ASCE/AHS/ASC Structures, Structural Dynamics and Materials Conference. AIAA 2012–1817. Honolulu, HI

Sobol′ I (2001) Global sensitivity indices for nonlinear mathematical models and their Monte Carlo estimates. Math Comput Simul 55: 271–280. https://doi.org/10.1016/S0378-4754(00)00270-6

Sobol IM (1990) Quasi-Monte Carlo methods. Prog Nucl Energy 24:55–61. https://doi.org/10.1016/0149-1970(90)90022-W

Sparkman DM, Garza JE, Millwater HR, Smarslok BP (2016) Importance sampling-based post-processing method for global sensitivity analysis. In: 18th AIAA Non-Deterministic Approaches Conference. AIAA 2016–1440. San Diego, CA

Terrell G, Scott D (1992) Variable kernel density estimation. Ann Stat 20: 1236–1265

West IV, Thomas K, Hosder S (2015) Uncertainty quantification of hypersonic reentry flows with sparse sampling and stochastic expansions. J Spacecr Rocket 52:120–133. https://doi.org/10.2514/1.A32947